arXiv:1602.00129v1 [physics.optics] 30 Jan 2016

Rapid, broadband spectroscopic temperature measurement of CO_2 using VIPA spectroscopy

Andrew Klose[1]‡

Gabriel Ycas[1]

Flavio C. Cruz[1,2]

Daniel L. Maser[1,3]

Scott A. Diddams[1,3]

[1] National Institute of Standards and Technology, Boulder, CO, USA 80305
[2] Instituto de Fisica Gleb Wataghin, Universidade Estadual de Campinas, Campinas, SP, 13083-859, Brazil
[3] Department of Physics, University of Colorado, Boulder, CO, USA 80309

E-mail: aklose@augie.edu

Abstract. Time-resolved spectroscopic temperature measurements of a sealed carbon dioxide sample cell were realized with an optical frequency comb combined with a two-dimensional dispersive spectrometer. A supercontinuum laser source based on an erbium fiber mode-locked laser was employed to generate coherent light around 2000 nm (5000 cm^{-1}). The laser was passed through a 12-cm-long cell containing CO_2, and the transmitted light was analyzed in a virtually-imaged phased array- (VIPA-) based spectrometer. Broadband spectra spanning more than 100 cm^{-1} with a spectral resolution of roughly 0.075 cm^{-1} (2.2 GHz) were acquired with an integration period of 2 ms. The temperature of the CO_2 sample was deduced from fitting a modeled spectrum to the line intensities of the experimentally acquired spectrum. Temperature dynamics on the time scale of milliseconds were observed with a temperature resolution of 2.6 K. The spectroscopically-deduced temperatures agreed with temperatures of the sample cell measured with a thermistor. Potential applications of this technique include quantitative measurement of carbon dioxide concentration and temperature dynamics in gas-phase chemical reactions (e.g., combustion), and plasma diagnostics.

‡ Present address: Department of Chemistry, Augustana University, Sioux Falls, SD, USA.

1. Introduction

Spectroscopic temperature measurements using coherent or incoherent light sources coupled to optical spectrometers have been accomplished by measuring the distribution amongst the quantized energy levels of a given sample, for example, the ro-vibrational intensities of a molecule [1]. Moreover, the dependence of the experimental spectrum on temperature and pressure is also observed via line-shape broadening and line-center shifts. The temperature and pressure of the system can be deduced by comparing the experimental spectrum to a modeled spectrum that includes temperature and pressure dependence. Spectroscopic temperature measurements based on sample absorption have several advantages compared to well-established temperature measurement tools such as thermocouples, thermistors, and blackbody radiation spectral measurements. For example, in an optical setup, light can be passed through a gas sample to measure the temperature *in situ*, and integrated across a remote path of the gas sample, as compared to a point measurement from a device mounted onto the container wall.

There has been much research into the development of spectroscopic temperature measurement sensors. Measurements with such systems have been accomplished by rapidly scanning (10 kHz to 1 MHz) single-frequency lasers over absorption features in sample gases in harsh environments to measure the linewidth, centroid, and intensity [2–4]. One disadvantage of previous spectroscopic temperature measurements is the tradeoff of spectral bandwidth for rapid scanning on time scales of under 1 ms. Specifically, using a single diode laser source, it has been difficult to achieve rapid spectroscopic measurement with spectral bandwidth of more than 15 cm^{-1}. However, in cases where sample absorption is weak, or where the sample is contained in an interfering matrix, it is advantageous to interrogate more sample absorption features by measuring over a larger optical bandwidth. Previously, Fourier-transform techniques have been used with much success for broadband measurements to monitor dynamic systems [5]. To achieve the desired time resolution in this case, the system under study must be readily reproducible and the spectrometer must be synced with "time-zero" of the event being studied [5]. Each desired Fourier stage position must be measured as a function of event time delay.

Here, the implementation of an optical frequency comb coupled to a two-dimensional spatially-dispersive spectrometer has been realized to measure temperature dynamics on time scales less than 10 ms in a single shot measurement. Individual spectra spanning more than 100 cm^{-1} with a spectral resolution of 0.075 cm^{-1} (2.2 GHz) were acquired with an integration period of 2 ms. The time between consecutive spectra was 8.3 ms, limited by the 120 Hz frame rate of the camera integrated into the spectrometer. Previously, a similar system was used to measure time-dependent concentrations of transient species in photo-induced chemical reactions involving free-radicals [6]. In the present work, a spectroscopic temperature measurement technique is demonstrated by observing ro-vibrational intensity changes in absorption spectra of a CO_2 sample during resistive heating of a sample cell. The $20012 \leftarrow 00001$ spectral band of CO_2 centered at 4977.830 cm^{-1} [7] was probed in the current measurements.

2. Experimental Setup

The laser light used for spectroscopy was produced via supercontinuum generation from the amplified output of a 250 MHz erbium fiber mode-locked laser. The performance of the laser system is described in detail elsewhere [8]. Here the system is briefly described. The output of the erbium oscillator was amplified and compressed in fiber to achieve 70 fs full-width at half maximum (FWHM) pulses with an average power of 350 mW and an optical spectrum that spanned roughly 1500 nm to 1600 nm. The femtosecond pulses were delivered to a highly nonlinear fiber in which the optical spectrum was broadened to a bandwidth that spanned from 1000 nm to 2200 nm. The long-wavelength portion of the optical spectrum from 1980 nm to 2050 nm (4880 cm^{-1} to 5050 cm^{-1}) was used for spectroscopy of CO_2. A representative optical spectrum from the laser system is presented in Figure 1. The fiber-coupled output light was directed though a sample followed by a spectrometer system shown schematically in Figure 2. The laser light was launched into free space and split into two paths using a 50:50 beam splitter. One path passed through a temperature controlled 12-cm-long sample cell that had uncoated ZnSe windows positioned at Brewster's angle relative to the incident laser light. The second optical path was a reference path that did not pass through the sample cell. The beams from each path were recombined, coupled into an optical fiber, and delivered to a virtually-imaged phased array- (VIPA-) based spectrometer [9, 10].

The fiber-coupled input to the spectrometer was launched into free-space and focused into a 1-mm-thick VIPA etalon (free spectral range (FSR) $\sim$ 51 GHz) using a cylindrical lens (f = 50 mm). The VIPA was tilted roughly 4 degrees from normal to the incident light. The highly-dispersed output from the VIPA had overlapping orders separated by the VIPA FSR. The light was impinged onto a reflective diffraction grating orientated orthogonal to the VIPA dispersion to separate the overlapping VIPA orders. The two-dimensionally dispersed light was imaged onto a InSb camera using an f = 250 mm spherical lens; roughly 1 pW per comb mode was incident on the camera. The InSb camera had an array of 640 $\times$ 512 pixels with a pixel pitch of 20 μm, had a maximum full frame rate of 120 Hz, and was cooled to 77 K using liquid nitrogen.

The InSb camera was triggered by an optical chopper that acted on both the sample beam path and reference beam path. The chopped light from the sample path was out of phase with the reference path. The trigger signal allowed for the sample and reference images to be interleaved during data acquisition. Such interleaving allowed for rapid normalization of each acquired spectrum and minimized fast time-dependent drifts of the experimental setup. A second reference was acquired when the gas cell was under vacuum. The vacuum-cell reference allowed for calibration of the static wavelength dependent difference (from, e.g., etalons) between the two beam paths in the sampling setup.

3. Results and Discussion

Consecutive camera images of light passing through the CO_2-filled sample cell and reference arm are presented in panels (a) and (b) of Figure 3, respectively. An image of the absorption of CO_2 was generated by subtracting the dark image from all other images, then dividing the CO_2 sample image by the consecutive reference arm measurement. A similarly divided image was obtained with the cell under vacuum.

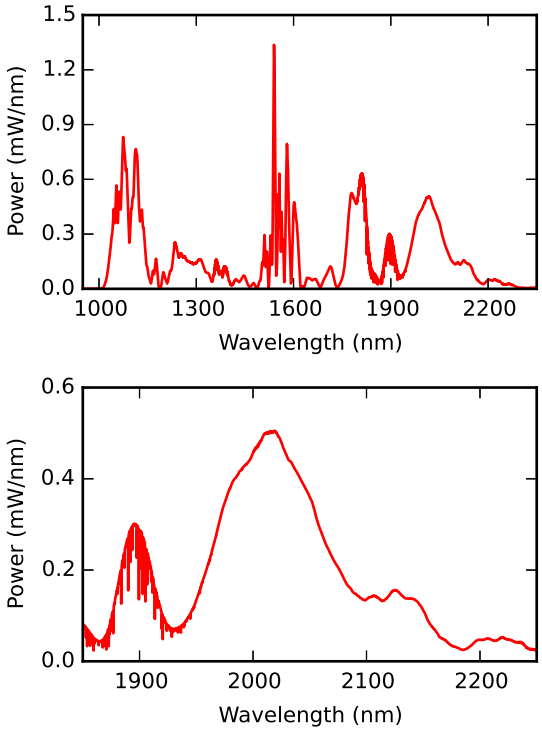

Figure 1. Example output supercontinuum spectrum from the Er mode-locked laser. The full spectrum is shown in the top panel, and an expanded view of the 2000 nm spectral region is presented in the bottom panel. Depletions near 1900 nm are due to water absorption in the spectrometer used for the measurement.

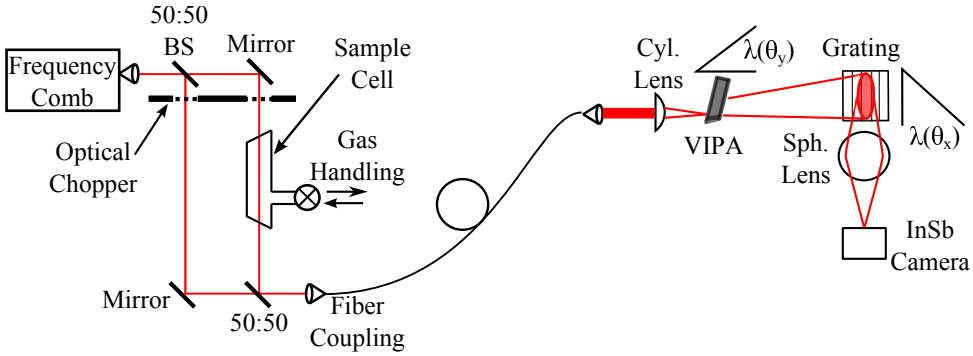

Figure 2. Schematic diagram of the experimental setup presented in the current work. Light from a mode-locked laser was split through two arms of the gas-cell measurement station, combined, and coupled into single mode fiber. The fiber-coupled light was delivered to the VIPA spectrometer, which is described in detail in the text. The reference signal from the optical chopper, which chopped both arms of the gas-cell measurement station, was used to sync the InSb camera in the spectrometer setup. The camera operated at 120 Hz and recorded interleaving images from each arm of the sampling setup.

The images were multiplied together as

$$\frac{I_{\mathrm{cell,CO2}}}{I_{\mathrm{ref,CO2}}} \times \frac{I_{\mathrm{ref,vac}}}{I_{\mathrm{cell,vac}}}, \tag{1}$$

where I denotes the image taken from the beam passing through the sample cell (cell) or reference path (ref) with CO_2 in the cell (CO2), or the cell under vacuum (vac). The two-step calibration minimized both short- and long-term wavelength-dependent drifts in the spectrometer. All images were acquired with a camera integration period of 2 ms per image. The CO_2 absorption is shown in panel (c) of Figure 3. The vertical stripes are due to the VIPA dispersion, and the free spectral range of the etalon was empirically determined by inspection of the camera image. The VIPA FSR is depicted as horizontal red lines in Figure 3. A typical transmission spectrum was constructed by appending consecutive stripes together to obtain a one-dimensional wavelength axis. The pixel intensity along each stripe is indicative of sample transmission.

The resolution of the spectrometer was measured to be (0.075 ± 0.003) cm^{-1}, or (2.2 ± 0.1) GHz, and was determined by launching a tunable single frequency external cavity diode laser (ECDL) into the spectrometer. The diode laser was scanned from 1980 nm to 2050 nm (4880 cm^{-1} to 5050 cm^{-1}) and camera images were recorded throughout the wavelength range. The resolution was consistent within 0.1 GHz throughout the portion of the image used to construct the line out spectrum. The limiting factor of the spectral resolution was the optical coatings on the VIPA etalon. The VIPA used in the present work was employed in previous measurements [11], and reflectance of the VIPA surfaces decreased above 2000 nm, limiting the finesse and ultimate resolution. However, the spectrometer presented here provided ample means to measure the absorption features of CO_2, which had broadened widths of more than 5 GHz.

Calibration of the frequency axis of the spectrum was done by fitting the pixel position of absorption peaks in the experimental spectrum to the peak positions of a modeled absorption spectrum obtained from the High Resolution Transmission (HITRAN) database [7]. A third-order polynomial fit of the experimental peak position to the modeled spectrum provided a hertz-per-pixel calibration of the experimental spectrum. After calibration, a least-squares fitting routine was used to achieve optimum agreement between the modeled and experimental spectra. In the minimization routine, the modeled spectrum, which is detailed in the appendix of Ref. [12], was allowed to vary in temperature and pressure. The path length through the CO_2 sample was fixed to 12 cm. The modeled absorbance spectrum was determined by calculating the line intensity from the number density and interaction length of the sample. A Voigt line shape was used in the model. The line shape accounted for pressure and temperature broadening, pressure shift of the line centroids, and temperature dependence of the line intensities [12]. While both temperature broadening and line intensities were simultaneously accounted for in the routine, the most sensitive effect for deducing the temperature from the fit was the dependence of each line intensity on temperature; the modest resolution of the present apparatus limited the observable effect of temperature broadening in the experimental spectra. Additionally, given the present resolution, line mixing and speed dependence of the line shape were not included in the model. The modeled spectrum was convolved with the instrument response, which was empirically determined from ECDL measurements to be well-approximated by a Gaussian function with a 2.2 GHz FWHM. A Lorentzian instrument response function, with a FWHM of 2.2 GHz, was used as response

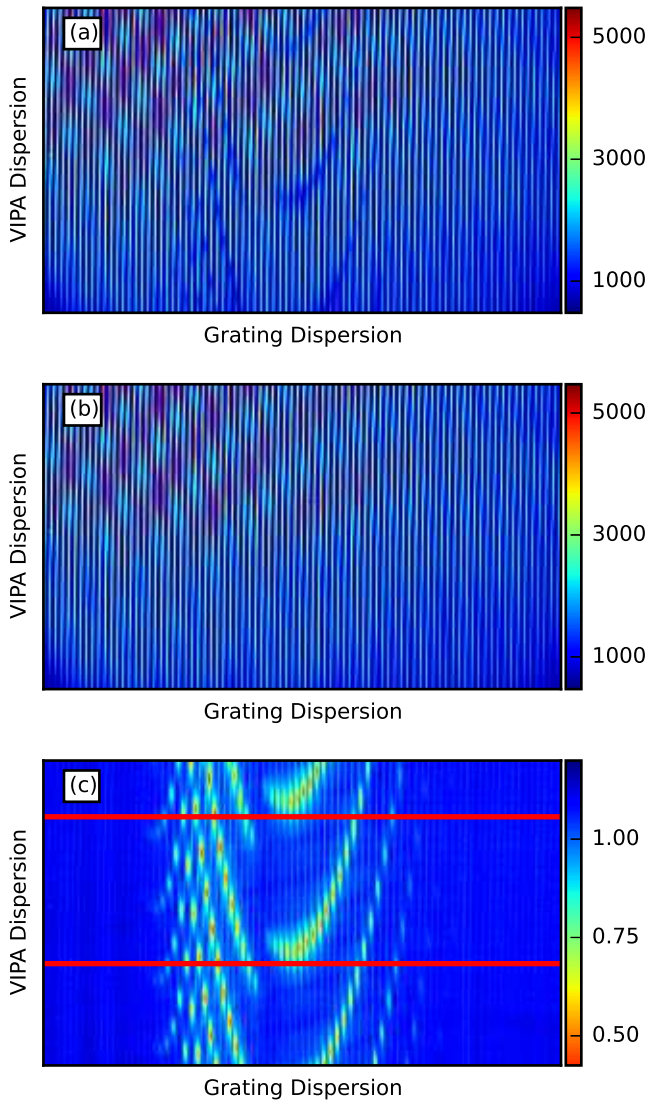

Figure 3. (a) Raw camera image of light passing through the CO_2-filled sample cell. (b) Raw camera image of light passing through the reference arm. Images presented in (a) and (b) were taken in consecutive camera frames. (c) Image of CO_2 absorption after image normalization described in the text. Red lines indicate the free spectral range of the VIPA.

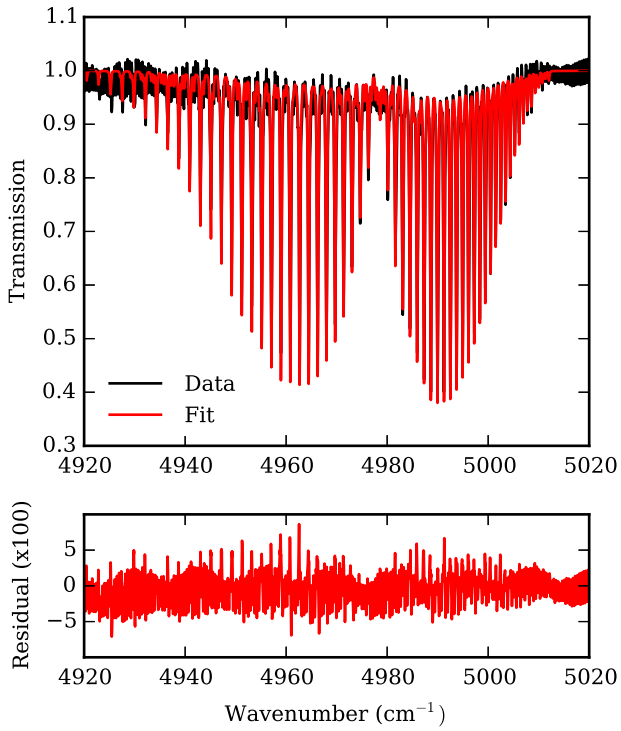

Figure 4. Fit result of a spectrum recorded when the measured temperature of the CO_2 cell was 328 K. The data and modeled spectrum are displayed on the upper panel, and the residuals are presented in the lower panel. The deduced temperature from the fit was 327 K.

function as well. The deduced temperature from the independent fits with the differing instrument response functions were consistent within the temperature uncertainty of 2.6 K, which is discussed later in the paper. After minimization, the frequency axis was re-calibrated using a third-order polynomial fit of the peaks in the experimental spectrum to peak positions of the optimum modeled spectrum obtained in the minimization routine. The alternating frequency calibration of the experimental spectrum and least-squares fitting of the modeled spectrum continued until the optimum modeled spectrum converged, which typically occurred after two iterations. A fit result is presented in Figure 4. Prior to measurement of the spectrum shown in Figure 4, the sample cell was measured to have a pressure of (700 ± 50) Torr and a temperature of (328 ± 3) K. The pressure and temperature deduced from the fit were 722 Torr and 327 K, respectively. The large uncertainty in measured pressure was a result of the use of an uncalibrated analog pressure transducer. Additionally, the transducer was mounted near, but not adjoining, the laser-interaction region, and the transducer was not at the same temperature as the interaction region. The pressures deduced from the fits agreed with the expected behavior as a function of increasing temperature (i.e. the ideal gas law), but further analysis of the uncertainty in the pressures deduced from the fits was not possible given the lack of a reliable truth measurement.

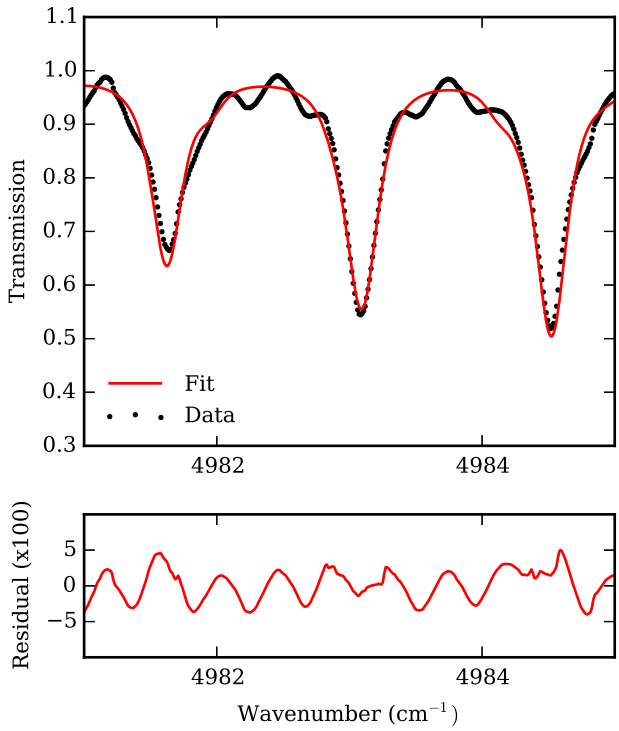

Figure 5. Zoomed in portion of a fit of the spectrum. The black dots indicate each vertical pixel moving along the vertical stripes from the VIPA image.

A zoomed in portion of the fit result is shown in Figure 5. The black dots in the figure indicate the signal from each pixel of the vertical stripes from the VIPA image. There was an etalon visible in the residual of the fit, and this effect was the limiting factor for the sensitivity of the deduced temperature in the present measurement. During the course of data collection, the etalon was minimized as much as possible. Because the goal in the present work was to fit spectra recorded with a single image, averaging multiple spectra to reduce the etaloning was not done. On the other hand, while analyzing the data, fitting, and alternatively Fourier filtering, of the etalon was attempted. However, these techniques were unsuccessful in removing the etalon because of small, but non-zero, non-linearities in the camera image-to-lineout spectrum conversion. Because of the non-linearities, the etalon did not have a single frequency and could not be removed or modeled successfully. In the future, if one wanted to increase the sensitivity of the measurement, fitting out, or better yet intrinsically reducing, the etalons would be optimal.

The spectrum presented in Figure 4 was one of a series of measurements where the cell was resistively heated and allowed to come to an equilibrium temperature. Spectra were acquired as a function of measured cell temperature. These spectra were fitted with modeled spectra [12], and the temperature of the gas was deduced from each fit. The deduced temperatures for each fit are plotted against the temperature measured with a thermistor in Figure 6. Uncertainty in the thermistor-measured

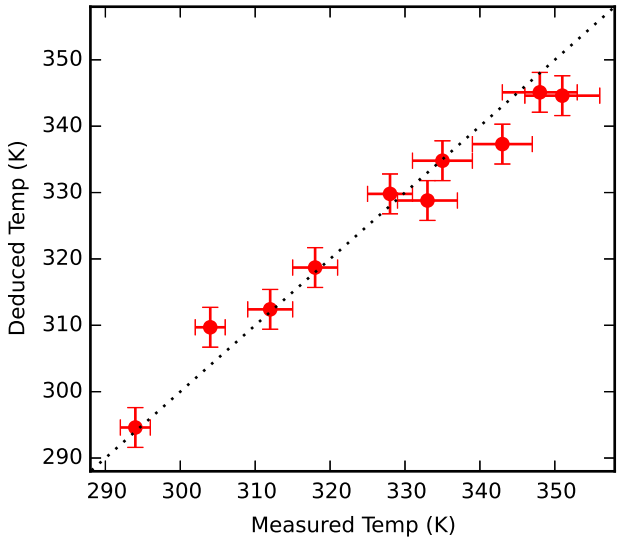

Figure 6. Comparison of spectroscopically-deduced (y axis) and thermistor-measured (x axis) temperatures over a 50 K range. The dotted black line is the curve $y = x$, not a fit.

temperatures was due to gradients present from uneven heating of the 12-cm-long cell. The reproducibility of the thermistor temperature measurements for a given heating set point was better than 1 K. Nonetheless, the deduced temperatures agree with the thermistor measurements over a range of over 50 K.

Dynamic temperature changes were investigated by resistively heating the cell to roughly 360 K, turning off the heating element, and recording CO_2 spectra over the course of ten minutes. Spectra were acquired every 13 s, with a camera integration period of 2 ms for each measurement. The temperature of the sample as a function of time was deduced by fitting each spectrum to the model described previously. The result of the time-dependent spectroscopic temperature measurements is presented as red circles in Figure 7. The open black squares represent temperature measurements of the cell using the thermistor. The temperature measurements, deduced from spectra that were acquired in 2 ms, agree with the thermistor-measured temperature over the 10 min time scale of the dynamic measurement. The thermistor-measured temperatures were fit with an exponential decay function; the result is plotted as a black line on Figure 7. The deviation of the spectroscopically-deduced temperatures from the exponential fit is presented as a histogram in Figure 8. The histogram was fitted with a Gaussian function, and the mean and FWHM of the fitted distribution were 1.4 K and 2.6 K, respectively. The 1.4 K accuracy of the deduced temperatures compared to exponential temperature decay fit is within the uncertainty of the sample-cell temperature.

More notably, the fit result in Figure 8 indicates that the uncertainty in the spectroscopically-deduced temperatures was 2.6 K. The change in uncertainty, or increase in sensitivity, was investigated here by deducing the sample temperature by fitting sub-sections of the full measured bandwidth. The 50 spectra acquired during the sample temperature decay were independently fitted multiple times with differing

numbers of absorption features in the spectrum. A total of 53 absorption features were visible above the background noise. The differing intensity of the absorption features was normalized by adding the maximum absorption of all of the peaks included in each fit. This sum gives an equivalent number of peaks, denoted N_{lines}, that absorb nearly 100 % of the incident light. A related approach using the integrated area peaks was considered in the case of gas mixing in the supplementary information of Ref [13]. In the present work, the standard deviation of the difference between the deduced temperatures and exponential decay fit are plotted as a function of the number of normalized absorption lines in Figure 9. The spectra were fitted in three separate sequences. First, the center of the spectrum was fitted, and additional peaks on each side were systematically included as the fitted spectral window was widened. The result from this sequence is presented as green circles in Figure 9. Second, the far red portion of the spectrum, near 4920 cm^{-1}, was fitted, and additional peaks with centroids at higher wavenumbers were systematically included as the fitting window was widened. Those data are presented as red squares in Figure 9. Third, the far blue portion of the spectrum, near 5000 cm^{-1}, was fitted, and additional peaks with centroids at lower wavenumbers were systematically included as the fitting window was widened; the result is presented as blue triangles in Figure 9. The behavior, regardless of the fitting window was consistent. The deviation is large, near 25 K for low values of N_{lines}, and saturates near 3 K for large values of N_{lines}. The saturation behavior is an indication that the temperature gradient across the cell may be a limiting factor in the sensitivity. Nonetheless, a temperature sensitivity of ± 2.6 K was achieved in the present case of a sample with roughly 50 peaks absorbing between 5 % and 60 % of the incident light. If the discrepancies of each peak intensity were random, it would be expected that the uncertainty would decrease as the square root of independent absorption features of equal intensity. The function $A_0/\sqrt{N_{\text{lines}}}$, where A_0 is a free parameter, was fitted to these data and is shown as a solid purple line in Figure 9. However, in the present case, the absorption for the CO_2 peaks are not independent, but rather are coupled for a given temperature. Thus, the uncertainty of the spectroscopically deduced temperature decreases faster as a function of equivalent peaks than the square-root function. The correlation can be modeled by adding in a term with $1/(N_{\text{lines}})$ dependence, namely by fitting the function $A_0/(N_{\text{lines}}) + A_1/\sqrt{N_{\text{lines}}}$, where A_0 and A_1 are free parameters, to the data. The fit of the two-term function, shown as the dashed black line in Figure 9, reproduces the trend in the data, and illustrates the correlation of fitting multiple spectral feature intensities. This result highlights another advantage of the simultaneous measurement of the full ro-vibrational band.

4. Conclusions

Rapid spectroscopic temperature measurements of a gaseous carbon dioxide sample were realized via absorption spectroscopy. An Er-based mode-locked laser was used to generate a supercontinuum spectrum, and light near 2000 nm (5000 cm^{-1}) was used to interrogate the CO_2 sample. The light was delivered to a VIPA-based two-dimensional dispersive spectrometer, which provided the means to record a sample transmission spectrum with more than 100 cm^{-1} bandwidth simultaneously with 2 ms of integration time. Deduced temperatures from line intensities allowed for the determination of the CO_2 sample temperature with an uncertainty of ± 2.6 K. Temperature dynamics on a time scale of ten minutes were measured with the present

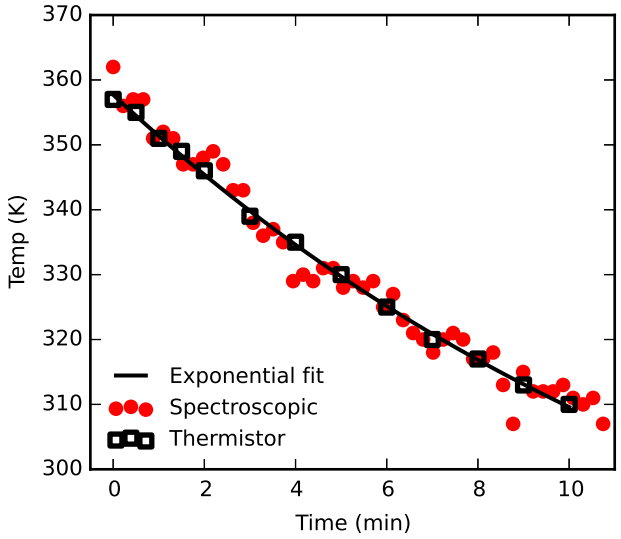

Figure 7. Temperature decrease of the CO_2 sample cell. The heating element was turned off at time zero of the plot. The black squares are thermistor measurements, and the red circles are spectroscopically-deduced temperatures. The solid black line is an exponential fit to the thermistor temperature measurements.

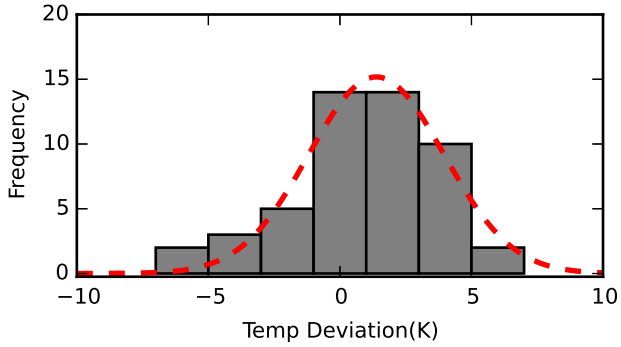

Figure 8. Histogram of the average deviation of spectroscopically-deduced temperature from the exponential fit of the temperature decay of the CO_2 cell presented in Figure 7. The dashed line is the fit of a Gaussian function to the histogram. The mean and FWHM of the Gaussian function were 1.4 K and 2.6 K, respectively.

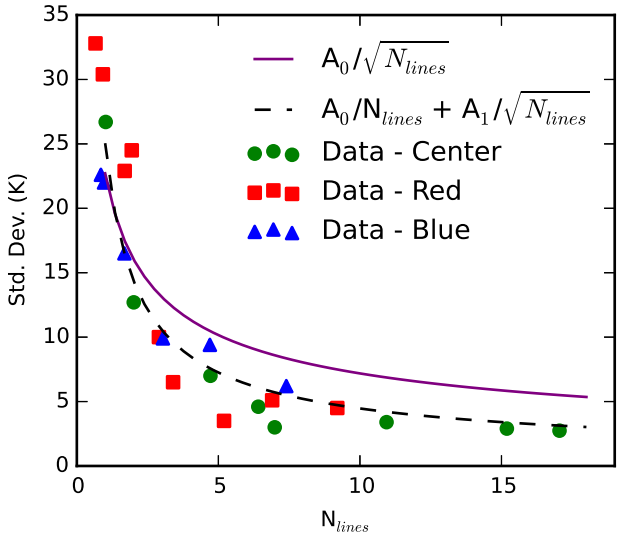

Figure 9. Standard deviation of spectroscopically-deduced temperatures as a function of the number of spectral features measured. $N_{\text{ lines}}$denotes a normalized quantity that is the effective number of absorption lines that attenuate nearly 100 % of the incident light. The independent data sets are described in the text. The solid purple and dashed black curves are fits of the functions $\left(A_0/\sqrt{N_{\text{ lines}}}\right)$ and $\left(A_0/N_{\text{ lines}} + A_1/\sqrt{N_{\text{ lines}}}\right)$ to the data, respectively.

system, and agreed with thermistor temperature measurements of the sample cell. It is intended to implement the present spectrometer to measure temperature dynamics of CO_2 in systems, such as photo-induced reactions, that change on time scales of milliseconds. It is possible to increase the frame rate of the InSb camera by reducing the image size acquired. This trade-off of faster acquisition may outweigh the reduction in measured optical bandwidth for some applications. Other frequency comb-based spectroscopic techniques, that do not require a liquied nitrogen-cooled InSb camera, may be advantageous for rapid spectroscopic temperature measurements as well. For example, implementation of a dual-comb spectroscopic setup [14–17] would allow for time resolution of less than 1 ms, but may require averaging of multiple shots. The implementation of these techniques will allow for rapid and broadband spectroscopic temperature measurements of dynamic systems.

Acknowledgments

This work was supported in part by the NIST Greenhouse Gas and Climate Science Measurements Program. The authors thank T.A. Johnson, L. Nugent-Glandorf, F. Quinlan, and F. Giorgetta for useful discussions, J. Ye for providing the VIPA etalon, and M. Hirano of Sumitomo for providing the nonlinear fiber. A.K. acknowledges support from the National Research Council Postdoctoral Fellowship Program, and F.C.C. acknowledges support from CNPq, Fapesp and NIST. This work is a contribution of the United States Government and is not subject to copyright in the United States.

References

[1] Ronald K. Hanson and Patricia Kuntz Falcone. Temperature measurement technique for high-temperature gases using a tunable diode laser. *Appl. Opt.*, 17(16):2477–2480, Aug 1978.

[2] Scott Sanders, Daniel Mattison, Lin Ma, Jay Jeffries, and Ronald Hanson. Wavelength-agile diode-laser sensing strategies for monitoring gas properties in optically harsh flows: application in cesium-seeded pulse detonation. *Opt. Express*, 10(12):505–514, Jun 2002.

[3] G. B. Rieker, H. Li, X. Liu, J. B. Jeffries, R. K. Hanson, M. G. Allen, S. D. Wehe, P. A. Mulhall, and H. S. Kindle. A diode laser sensor for rapid, sensitive measurements of gas temperature and water vapour concentration at high temperatures and pressures. *Meas. Sci. Technol*, 18:1195, 2007.

[4] A. Lytkine, W. Jäger, and J. Tulip. Tunable diode laser spectroscopy of ethylene oxide near 1693 nm. *Applied Physics B*, 98(4):871–876, 2010.

[5] Eric L. Woodbridge, T. Rick Fletcher, and Stephen R. Leone. Photofragmentation of acetone at 193 nm: rotational- and vibrational-state distributions of the carbon monoxide fragment by time-resolved FTIR emission spectroscopy. *The Journal of Physical Chemistry*, 92(19):5387–5393, 1988.

[6] Adam J. Fleisher, Bryce J. Bjork, Thinh Q. Bui, Kevin C. Cossel, Mitchio Okumura, and Jun Ye. Mid-infrared time-resolved frequency comb spectroscopy of transient free radicals. *The Journal of Physical Chemistry Letters*, 5(13):2241–2246, 2014.

[7] L.S. Rothman, I.E. Gordon, A. Barbe, D.Chris Benner, P.F. Bernath, M. Birk, V. Boudon, L.R. Brown, A. Campargue, J.-P. Champion, K. Chance, L.H. Coudert, V. Dana, V.M. Devi, S. Fally, J.-M. Flaud, R.R. Gamache, A. Goldman, D. Jacquemart, I. Kleiner, N. Lacome, W.J. Lafferty, J.-Y. Mandin, S.T. Massie, S.N. Mikhailenko, C.E. Miller, N. Moazzen-Ahmadi, O.V. Naumenko, A.V. Nikitin, J. Orphal, V.I. Perevalov, A. Perrin, A. Predoi-Cross, C.P. Rinsland, M. Rotger, M. imekov, M.A.H. Smith, K. Sung, S.A. Tashkun, J. Tennyson, R.A. Toth, A.C. Vandaele, and J. Vander Auwera. The HITRAN 2008 molecular spectroscopic database. *Journal of Quantitative Spectroscopy and Radiative Transfer*, 110(910):533 – 572, 2009.

[8] Andrew Klose, Gabriel Ycas, Daniel L. Maser, and Scott A. Diddams. Tunable, stable source of femtosecond pulses near 2 μm via supercontinuum of an erbium mode-locked laser. *Opt. Express*, 22(23):28400–28411, Nov 2014.

[9] M. Shirasaki. Large angular dispersion by a virtually imaged phased array and its application to a wavelength demultiplexer. *Opt. Lett.*, 21(5):366–368, Mar 1996.

[10] Scott A. Diddams, Leo Hollberg, and Vela Mbele. Molecular fingerprinting with the resolved modes of a femtosecond laser frequency comb. *Nature*, 445:627–630, Feb 2007.

[11] K.C. Cossel, F. Adler, K.A. Bertness, M.J. Thorpe, J. Feng, M.W. Raynor, and J. Ye. Analysis of trace impurities in semiconductor gas via cavity-enhanced direct frequency comb spectroscopy. *Applied Physics B*, 100(4):917–924, 2010.

[12] L.S. Rothman, C.P. Rinsland, A. Goldman, S.T. Massie, D.P. Edwards, J-M. Flaud, A. Perrin, C. Camy-Peyret, V. Dana, J.-Y. Mandin, J. Schroeder, A. McCann, R.R. Gamache, R.B. Wattson, K. Yoshino, K.V. Chance, K.W. Jucks, L.R. Brown, V. Nemtchinov, and P. Varanasi. The HITRAN molecular spectroscopic database and HAWKS (HITRANN Atmospheric Workstation): 1996 edition. *Journal of Quantitative Spectroscopy and Radiative Transfer*, 60(5):665 – 710, 1998.

[13] Florian Adler, Piotr Masłowski, Aleksandra Foltynowicz, Kevin C. Cossel, Travis C. Briles, Ingmar Hartl, and Jun Ye. Mid-infrared fourier transform spectroscopy with a broadband frequency comb. *Opt. Express*, 18(21):21861–21872, Oct 2010.

[14] Fritz Keilmann, Christoph Gohle, and Ronald Holzwarth. Time-domain mid-infrared frequency-comb spectrometer. *Opt. Lett.*, 29(13):1542–1544, Jul 2004.

[15] Ian Coddington, William C. Swann, and Nathan R. Newbury. Coherent multiheterodyne spectroscopy using stabilized optical frequency combs. *Phys. Rev. Lett.*, 100:013902, Jan 2008.

[16] Philippe Giaccari, Jean-Daniel Deschênes, Philippe Saucier, Jerome Genest, and Pierre Tremblay. Active Fourier-transform spectroscopy combining the direct RF beating of two fiber-based mode-locked lasers with a novel referencing method. *Opt. Express*, 16(6):4347–4365, Mar 2008.

[17] G. B. Rieker, F. R. Giorgetta, W. C. Swann, J. Kofler, A. M. Zolot, L. C. Sinclair, E. Baumann, C. Cromer, G. Petron, C. Sweeney, P. P. Tans, I. Coddington, and N. R. Newbury. Frequency-comb-based remote sensing of greenhouse gases over kilometer air paths. *Optica*, 1(5):290–298, Nov 2014.